ENHANCING THE SIGNAL-TO-NOISE RATIO OF SONIC LOGGING WAVEFORMS BY SUPER-VIRTUAL INTERFEROMETRIC STACKING

ALI A. DAWOOD, ABDULLATIF AL-SHUHAIL and
ABDULRAHMAN ALSHUHAIL

Saudi Aramco, Office 208 Bldg. 137, Dhahran, 31311, Saudi Arabia
ali.dawood.18@aramco.com

(Received June 23, 2019; revised version accepted October 14, 2020)

ABSTRACT

Dawood, A.A., Al-Shuhail, A. and Alshuhail, A., 2021. Enhancing the signal-to-noise ratio of sonic logging waveforms by super-virtual interferometric stacking. *Journal of Seismic Exploration*, 30: 237-255.

Sonic logs are essential tools for reliably identifying interval velocities, which, in turn, are used in many seismic processes. Borehole irregularities and washout zones along the borehole surface can cause the signal-to-noise ratio of recorded sonic waveforms to be quite low. Noisy borehole conditions can decrease the signal-to-noise ratio and mask the signal recorded by the receiver stations. To mitigate this problem, we have extended the theory of super-virtual refraction interferometric stacking to enhance the signal-to-noise ratio of sonic waveforms. This theory is composed of two redatuming steps followed by a stacking operation. The first redatuming procedure is of correlation type, where sonic waveforms are correlated with each other to obtain virtual waveforms with the sources datumed to the refractor. The second datuming step is of convolution type, where virtual sonic waveforms are convolved with the recorded waveforms to de-datum the sources back to their original positions. The stacking procedure following each step enhances the signal-to-noise ratio of the refracted P-wave first arrivals. Datuming with correlation and convolution of traces introduces spurious events known as correlation artifacts in the super-virtual dataset. To overcome this problem, we replace the correlation-type datuming step by a deconvolution-type datuming step. Although the cross-correlation-based datuming method is more robust, the deconvolution-based datuming method significantly suppresses the spurious artifacts. To limit the noise amplification effect caused by the deconvolution step, we add a non-zero regularization parameter to stabilize the deconvolution of the virtual sonic waveforms. Our tests on synthetic and real data examples show remarkable signal-to-noise ratio enhancement of refracted P-wave arrivals in the sonic waveforms. These tests further demonstrate how the use of deconvolution-type datuming instead of the conventional correlation-type datuming may significantly suppress the correlation artifacts. The semblance analysis demonstrated that the super-virtual sonic waveforms yields more robust formation velocities compared to the raw waveforms.

KEY WORDS: Interferometry, Redatuming, Cross-Correlation, Convolution, Sonic

0963-0651/21/$5.00

INTRODUCTION

Sonic velocity logs are frequently used to estimate the properties of subsurface layers such as porosity and permeability. They are also used to tie the logging datasets with seismic data and core measurements (Goldberg et al., 2008). Therefore, accurate estimation of the compressional, shear, and Stoneley sonic velocities from sonic logging waveforms is essential to better utilize sonic logs. The goal of the acoustic logging tool is to estimate the formation slowness (i.e., velocity inverse) from the P-wave first breaks in sonic waveforms (Khadhraoui, 2011). One of the major challenges of sonic waveforms is the attenuation and dispersion of the acoustic waves traveling through the borehole fluid and rock matrix due to the internal particle friction within the medium, acoustic impedance changes, and borehole irregularities (Guerin and Goldberg, 2002, 2005; Milani et al., 2015). Therefore, enhancing the first arrivals of sonic waveforms is an important challenge, especially when estimating the sonic velocity log in subsurface formations with low signal-to-noise ratio waveforms.

Seismic interferometry, also known as Green's function retrieval by cross-correlation, is widely used to redatum seismic sources and/or receivers from one position to another source/receiver position without knowledge of the underlying velocity model. Interferometric transformations are based on the cross-correlations, or convolutions of the recorded seismic traces, which act as natural wavefield extrapolators (Wapenaar and Fokkema, 2006; Schuster, 2009). One may also use this approach to extract the impulse response between receivers by making suitable combinations of the wavefields recorded at these receivers from different sources (Snieder et al., 2006). Bharadwaj et al. (2012) developed a data-driven interferometric technique, known as the super-virtual refraction interferometry (SVRI) theory, to enhance the post-critically refracted seismic energy. The proposed method is composed of two datuming steps followed by a stacking process:

1. A cross-correlation transformation to redatum the sources from the earth surface down to the refractor followed by a stacking step.

2. A convolution transformation to de-datuming the sources back to their original position followed by another stacking step.

Alshuhail et al. (2012) demonstrated the applicability of the super-virtual refraction interferometry theory to enhance P-wave first arrivals obtained using seismic reflection acquisition geometry in Saudi Arabia. Mallinson et al. (2011) demonstrated how SVRI can be used to enhance the imaging and extend the aperture of refractors by introducing virtual traces with higher signal-to-noise ration (SNR). Recently, Al-Hagan et al. (2014) expanded the SVRI method and applied it using an iterative procedure to further enhance the first breaks via a combined correlation-convolution

framework. Gao and Zhang (2015) applied the super-virtual refraction interferometry to solve a 3D statics problem. They obtained the stationary source-receiver pair by an integral long source or receiver line without the requirement of knowing the stationary locations.

Redatuming with cross-correlation causes wavelet distortion and introduces spurious events in the virtual gathers, known as the correlation artifacts, which may yield to the wrong identification of the desired events (Alshuhail et al., 2012). An et al. (2014) utilized an inverse correlation function to enhance the quality of the near-offset traces, and a wavelet shaping function to suppress the spurious events in the super-virtual gather due to the cross-correlation and convolution steps applied in the super-virtual refraction interferometry. To suppress the spurious artifacts in interferometric redatuming, deconvolution (i.e., spectral division of the two traces) could be utilized instead of the cross-correlation of the two traces to obtain the virtual response (Vasconcelos and Snieder, 2008; Wapenaar et al., 2011). In the presence of highly variable and strong additive noise, cross-coherence datuming (Chavez-Garcia and Luzon, 2005; Bendat and Piersol, 2011), which applies the normalization by the spectral amplitude of each trace, could be used instead of the cross-correlation or deconvolution to suppress the noise influence (Bensen et al., 2007; Nakata et al., 2011).

In this work, we extend the application of the super-virtual seismic refraction interferometry theory to include the refracted wavefield in sonic waveforms. For reflection-type interferometry, a Fresnel zone (i.e., region of stationary points) around the stationary point needs to be sampled densely to construct a virtual reflection event (Schuster et al., 2004; Snieder, 2004). Snieder et al. (2008) showed that the dominant contribution to the interferometric summation comes from this stationary phase region. Sparse distribution of either sources or receivers often causes poor illuminations of the desired virtual responses, and gives rise to the appearance of spurious artifacts due to the incomplete addition and cancellation in the stationary-phase region (Ruigrok et al., 2010). It has been shown that the extraction of body waves by cross-correlation of noise is more difficult than of surface waves (Draganov et al., 2009; Nakata et al., 2011) as the stationary phase regions of surface waves are much larger than the ones for body waves (Forghani and Snieder, 2010).

The refraction events are excellent candidates for interferometric transformation as their common ray paths grazes the boundary between two layers and travel with the faster speed of the underlying formation. As a result, the interferometric summation is rich with stationary phase contributions. Thus, the refractors can be illuminated by a smaller number of physical sources and receivers using the SVRI method such as the refracted sonic waveforms. SVIR aims to enhance the noisy far offset refraction energy by stacking over stationary source, and virtual receiver positions.

However, the near-offset traces are weakened as the associated stationary points are only partly sampled (Ruigrok et al., 2010).

Our goal is to test the possibility of enhancing the signal-to-noise ratio of sonic waveforms in both synthetic and real data examples. We further modify the super-virtual interferometric stacking method by replacing the cross-correlation datuming step by a cross-coherence or deconvolution datuming step. Our objective is to suppress the spurious events (i.e., correlation artifacts), enhance the temporal resolution of the super-virtual waveforms, and properly deconvolve the source wavelet. We finally apply the modified super-virtual interferometric stacking method to mitigate the artifacts and enhance the temporal resolution of synthetic and field sonic waveforms.

SUPER-VIRTUAL REFRACTION INTERFEROMETRY

The theory of super-virtual (SV) refraction interferometry is based on two redatuming steps. The first datuming step utilizes the far-field approximation of the reciprocity equation of correlation type in the frequency domain (Wapenaar and Fokkema, 2006):

$$Im\left[G(B|A)^{virtual}\right] = k \int_{S_0} G(A|W)^{*} G(B|W) dW \quad , \tag{1}$$

where $G(A|W)^{*}$ is the recorded sonic waveform recorded at A due to a transmitting source at W. $G(B|W)$ is the complex conjugate of the recorded sonic waveform recorded at B due to a transmitting source at W. $G(B|A)^{virtual}$ is the resultant Green's function and its time-reversed version recorded by a receiver at B due to a virtual source placed at Y, which is schematically shown in Fig. 1. Note that the virtual source at Y has been redatumed to the formation at the point where the rays from the original source W to the receivers A and B diverge. Therefore, the cross-correlation step annihilates the common propagation path and the traveltimes associated with the common raypath subtract. Also, note that the resultant virtual sonic waveform has a negative excitation time, denoted by the dashed ray, equals to the time it takes the refracted wave to travel from A to Y. S_0 is the integration surface shown in Fig. 1, where we sum the cross-correlated waveforms over all possible sources W's, and k is the wavenumber. The summation surface allows the stacking of up to (r–1) virtual responses, where r is the number of receivers in the tool. Therefore, the increase of the signal-to-noise ratio is higher for far offset shots than near-offset shots.

A mute function should be applied to window around the refracted arrivals prior to the cross-correlation step (Al-Hagan et al., 2014). This is an essential step to suppress the correlation artifacts and to prevent the undesired correlation of refractions with direct arrivals, reflections, and/or

surface waves with dominant stationary phase regions. This resembles the windowing operation is performed for VSP data (Yu and Schuster, 2004) or seismic data in general (Snieder et al., 2008). In the case of sonic waveforms, we aim to suppress artifacts caused by the correlation of refractions with mode-converted modes, and Stoneley waves.

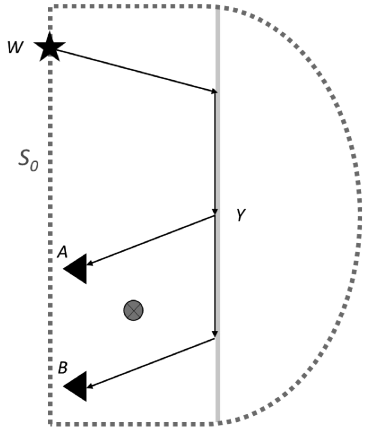

a) Correlation-type datuming.

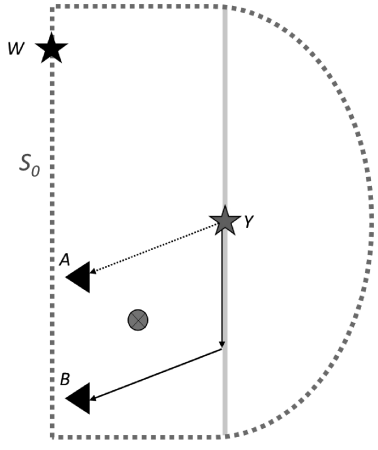

b) Virtual sonic waveform.

Fig. 1. Schematic ray diagrams for correlation-type datuming: a) Correlating the sonic waveform fired at *W* and received at *B* with the sonic waveform fired at *W* and received at *A*. b) The resultant virtual sonic waveform due to a virtual shot placed at point *Y* on the formation and a receiver at *B*. This waveform has a negative excitation time equals to the time it takes the refracted wave to travel from *A* to *Y*, denoted by the dashed ray.

The virtual sonic waveform $G(B|A)^{virtual}$ often suffers from wavelet distortion, low temporal resolution, and spurious correlation artifacts. These effects are caused by the imperfect summation in eq. (1) due to the limited recording aperture along the vertical borehole and the cross-correlation of the seismic traces. Classically, the redatuming is performed using the cross-correlation of the waveforms in interferometric transformations (Wapenaar et al., 2010):

$$G(B|A)^{virtual} = G(A|W)^{*}G(B|W) \quad , \tag{2}$$

Vasconcelos and Snieder (2008) proposed datuming with deconvolution to suppress the source function, and mitigate the effect of the cross-correlation artifacts:

$$G(B|A)^{virtual} = \frac{G(B|W)}{G(A|W)} = \frac{G(B|W)G(A|W)^{*}}{G(A|W)G(A|W)^{*}} \quad . \tag{3}$$

While both datuming methods in eqs. (2) and (3) subtract the phases (i.e., traveltimes), the deconvolution datuming further divides the color (i.e., account for the amplitude) as shown by Claerbout (1992). Therefore, one could incorporate the datuming with deconvolution instead of cross-correlation in the first step of the SVRI theory as follows:

$$G(B|A)^{virtual} = k \int_{S_0} \frac{G(B|W)\, G(A|W)^{*}}{G(A|W)\, G(A|W)^{*}+\epsilon} dW \quad , \tag{4}$$

where $\epsilon > 0$ is a regularizing small scalar to stabilize the spectral division as it prevents division by zeros. The value of ϵ is chosen on a trial-and-error basis. While a large real value of the regularizing scalar yields a cross-correlation datuming step, a small ϵ value yields a deconvolution datuming step. Similarly, Nakata et al. (2011) proposed datuming with cross-coherence instead of the classical cross-correlation of the waveforms, which can be utilized as the first datuming step in the SVRI method as follows:

$$G(B|A)^{virtual} = k \int_{S_0} \frac{G(B|W)\, G(A|W)^{*}}{|G(B|W)|\, |G(A|W)| + \epsilon} dW \quad . \tag{5}$$

The second datuming step in SVRI theory is a convolutional transformation to de-datum the sources from their virtual positions at the refractor back to their original positions. This step utilizes the far-field approximation of the reciprocity equation of convolution type in the frequency domain (Wapenaar et al., 2010), which is given by:

$$G(B|W)^{super} = 2ik \int_{S_1} G(B|A)^{virtual}\, G(A|W) dA \quad , \tag{6}$$

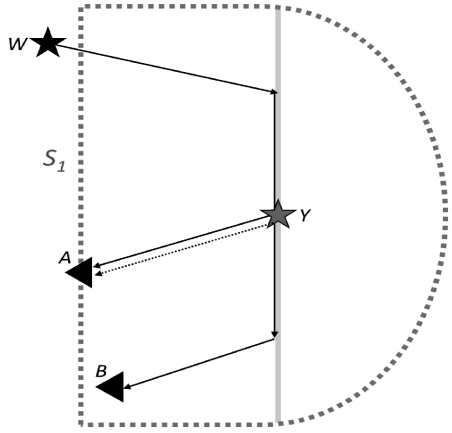

a) Convolution-type datuming

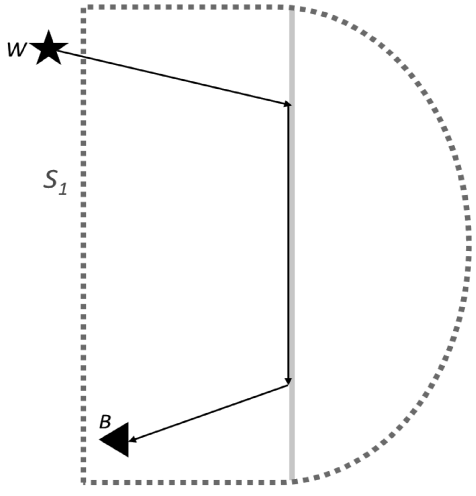

b) Super-virtual sonic waveform

Fig. 2. Schematic ray diagrams for convolution-type datuming: a) Convolving the sonic waveform fired at *W* and received at A with the virtual sonic waveform fired at *Y* and received at *B*. The negative excitation traveltime of the virtual waveform, denoted by the dashed ray, is annihilated by the positive traveltime of the original waveform, denoted by the solid ray. b) The resultant super-virtual waveform due to a source at *W* and recorded at receiver *B*.

where $G(B|W)^{super}$ is the super-virtual waveform, which is constructed by convolving an original waveform fired at W and received at A,$G(A|W)$, with the virtual trace $G(B|A)^{virtual}$ as illustrated schematically in Fig. 2. As a result, the negative excitation time (i.e., dashed ray from A to Y) is annihilated by the positive excitation time (i.e., solid ray from Y to A), and the source is redatumed back from the formation to its original position in the sonic tool. Note that the summation surface is now S_1, where we sum the data over the virtual source positions A's as shown in Fig. 2. This allows the stacking of up to (r–1) super-virtual responses, where r is the number of receivers in the tool. We next test the various datuming methods in applying the super-virtual refraction interferometric stacking procedure to enhance the signal-to-noise ratio of both synthetic and field data examples.

SYNTHETIC DATA EXAMPLE

The true velocity model used to generate the synthetic sonic waveforms is shown schematically in Fig. 3a. The velocity model consists of two layers: a hard formation with a P-wave velocity of 5000 m/s, and a borehole fluid with a P-wave velocity of 1500 m/s. The acquisition geometry consists of a transmitter (red star) and eight receivers equally spaced at 0.5 ft intervals (on the white line). The distance from the transmitter to the first receiver is 9 ft. The tool is moved in the uphole direction 8 times by 0.5 ft increments, and the transmitter is fired at each increment. The source is a Ricker wavelet, rotated by 90º, and has a dominant frequency of 10 kHz. The time sampling rate of the recorded sonic waveforms is 10 microseconds. We generated synthetic sonic waveforms using a second-order finite-difference solution to the acoustic wave equation. A typical noise-free common shot gather is plotted in Fig. 3b, and it shows the refracted P-wave first arrivals.

To simulate the effect of noisy borehole conditions and irregularities, we add random Gaussian white noise. We use a bandpass filter to limit the sonic waveforms to the sonic data bandwidth between 3-30 kHz. The noisy dataset is shown in Fig. 4a, and has a quite low SNR of 1.25, representing noisy borehole conditions. Note that the noise is masking the waveforms. The SNR is obtained by calculating the square of the amplitude ratio of the signal to noise. We apply the conventional correlation-convolution SVRI method to the synthetic sonic waveforms (Fig. 4b). As a result, the signal-to-noise ratio of the super-virtual dataset is increased to 9. Fig. 4b shows that the P-wave first arrivals becomes more pronounced in the super-virtual waveforms. Note that although the SNR has been increased by the super-virtual interferometric stacking, the method yields a super-virtual dataset, which is contaminated by correlation artifacts.

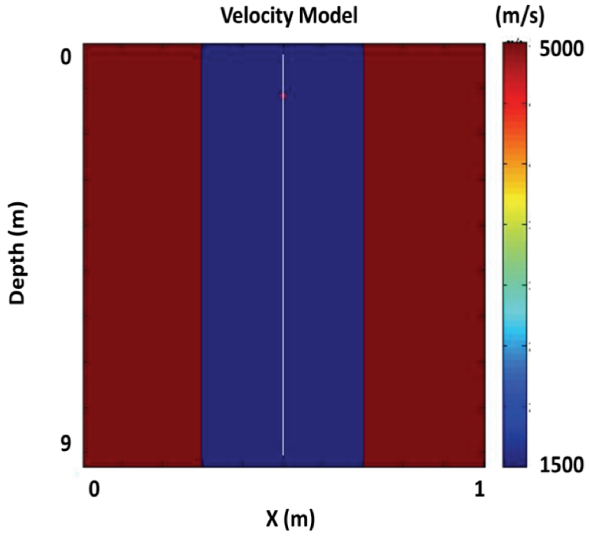

a) Synthetic velocity model.

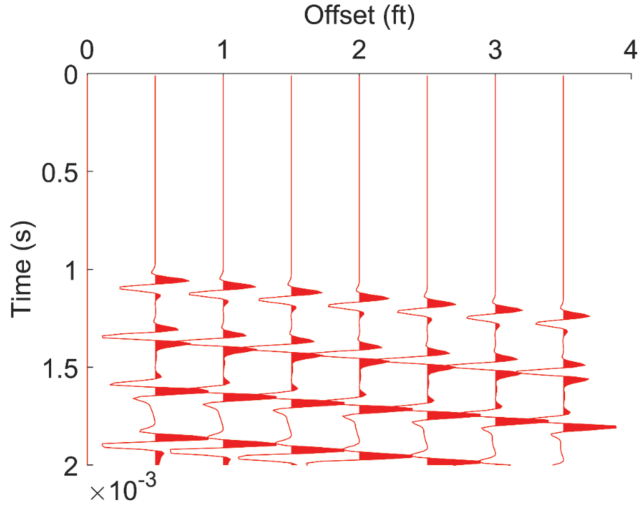

b) Noise-free sonic waveforms.

Fig. 3. Finite-difference modeling: a) The true velocity model. b) A typical noise-free common shot gather of sonic waveforms.

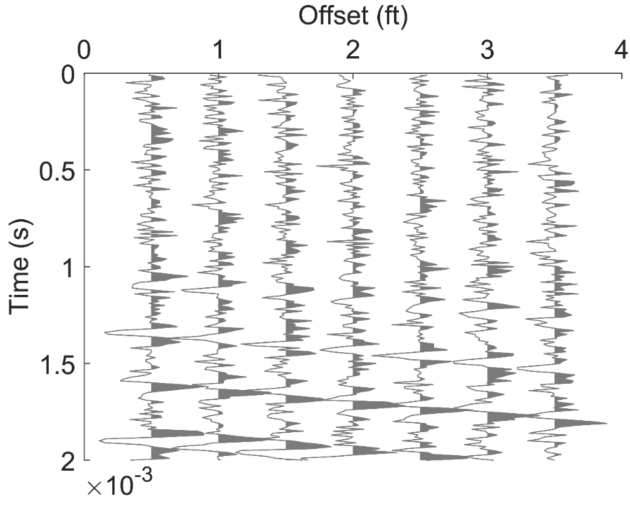

a) Noisy sonic waveforms

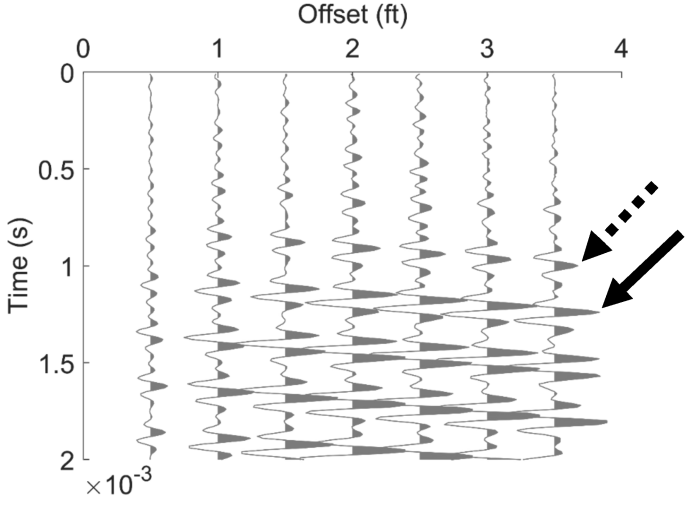

b) Super-virtual sonic waveforms using cross-correlation

Fig. 4. Synthetic SVRI sonic waveforms: a) Noisy sonic waveforms with SNR of 1.25. b) Super-virtual sonic waveforms using cross-correlation. The SNR is calculated to be 9. Note that the dashed arrow points to the spurious events caused by the cross-correlation and the solid arrow points to the actual first arrivals of P-wave sonic waveforms.

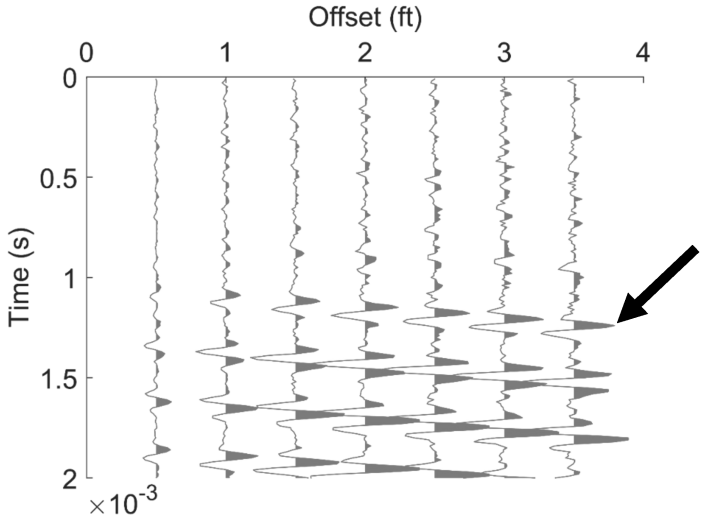

a) Super-virtual sonic waveforms using deconvolution.

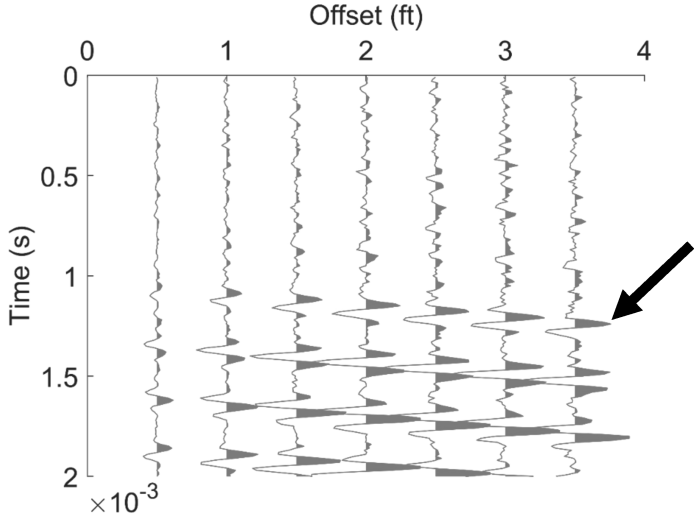

b) Super-virtual sonic waveforms using cross-coherence

Fig. 5. Synthetic SVRI sonic waveforms: a) Super-virtual sonic waveforms using deconvolution with SNR of 7. b) Super-virtual sonic waveforms using cross-coherence. The SNR is calculated to be 7.6. Note that the solid arrows point to the sonic P-wave first arrivals. The correlation artifacts are suppressed when redatuming using deconvolution and cross-coherence.

To alleviate the spurious events and suppress the correlation artifacts, we apply the modified super-virtual refraction interferometry method, where we perform datuming with deconvolution as in eq. (4) instead of cross-correlation in eq. (1). The super-virtual sonic waveforms with deconvolution is plotted in Fig. 5a, and it shows the suppression of the spurious events. The SNR of the deconvolved super-virtual dataset is calculated to be ~ 7.0. We also use datuming with cross-coherence in eq. (5) when applying the super-virtual interferometric stacking. Fig. 5b shows the super-virtual sonic waveforms obtained using cross-coherence, and it demonstrates the ability of the cross-coherence datuming to suppress the artifacts in the super-virtual gathers. The resultant super-virtual dataset has a SNR of 7.6. Despite the low SNR of the SVRI datasets obtained by deconvolution and cross-coherence compared with conventional cross-correlation SVRI data, the suppression of the spurious events would yield more accurate estimation of the sonic velocities.

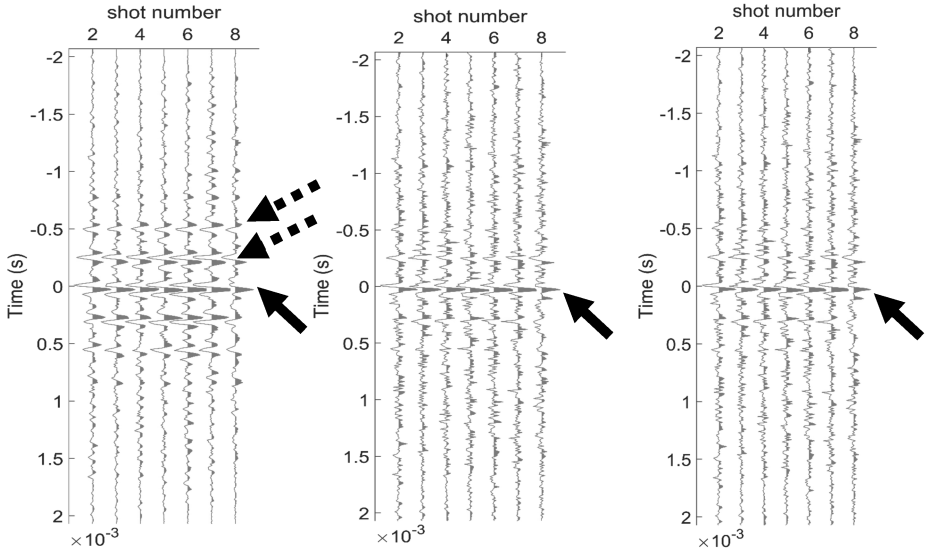

a) Cross-correlatinon datuming b) Deconvoltuion datuming c) Cross coherence datuming

Fig. 6. Synthetic cross-correlograms after the first datuming step by: a) cross-correlation, b) deconvolution, and c) cross-coherence. The summation surface S_0 is over all the contributing shots. The actual first-arrival sonic waveforms after the datuming is marked by the black arrow. The dashed arrow marks the spurious artifacts that appears due to the cross-correlation datuming step, which are suppressed by the deconvolution or cross-coherence datuming

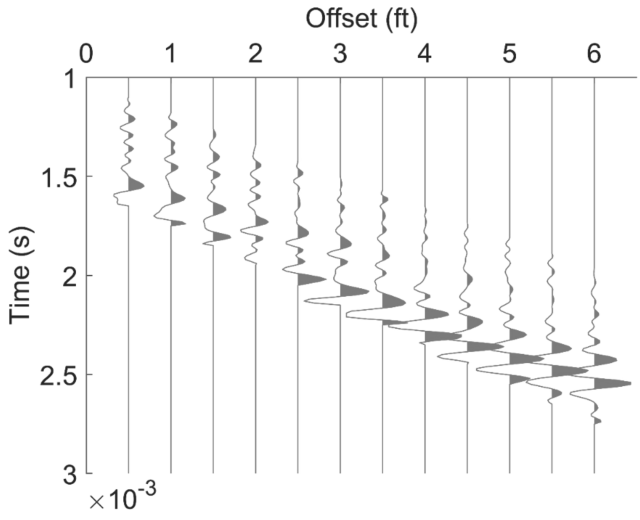

a) Noisy sonic waveforms

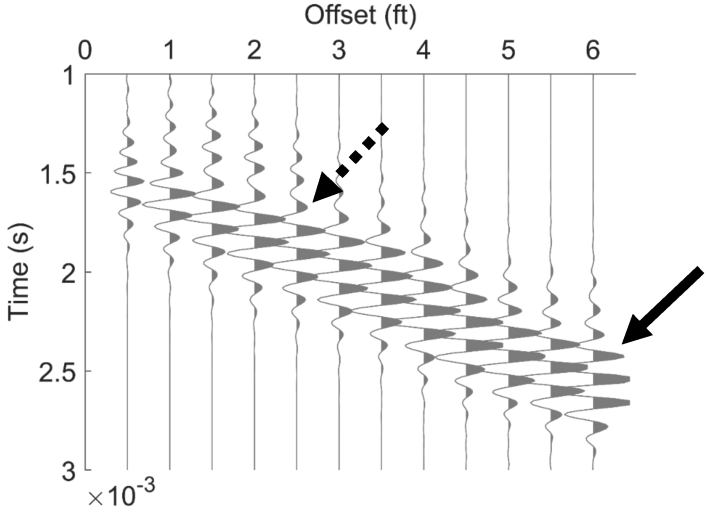

b) Super-virtual sonic waveforms using cross-correlation

Fig. 7. Field sonic data: a) Noisy sonic waveforms. b) SVRI sonic waveforms with cross-correlation. The noise level obscures the P-wave first arrivals. The first arrival signals in the SVRI sonic waveforms are enhanced compared with the noisy ones, especially for the far-offset stations. The solid arrow marks the sonic P-wave first arrivals and the dashed arrow points to the spurious events due to the cross-correlation datuming step.

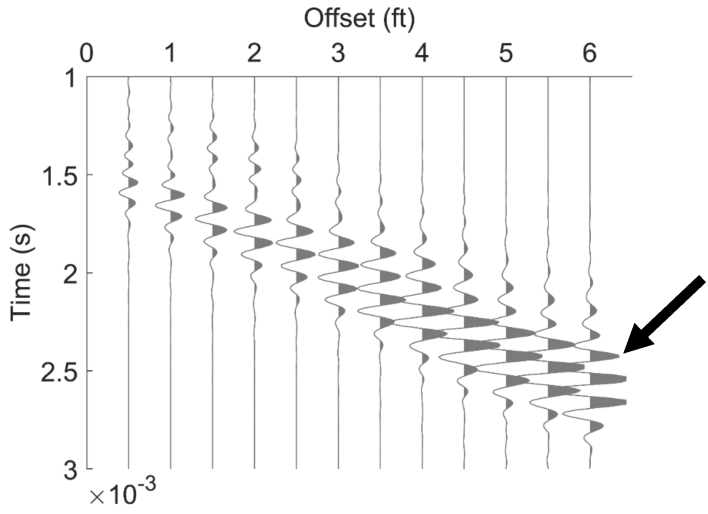

a) Super-virtual sonic waveforms using deconvolution

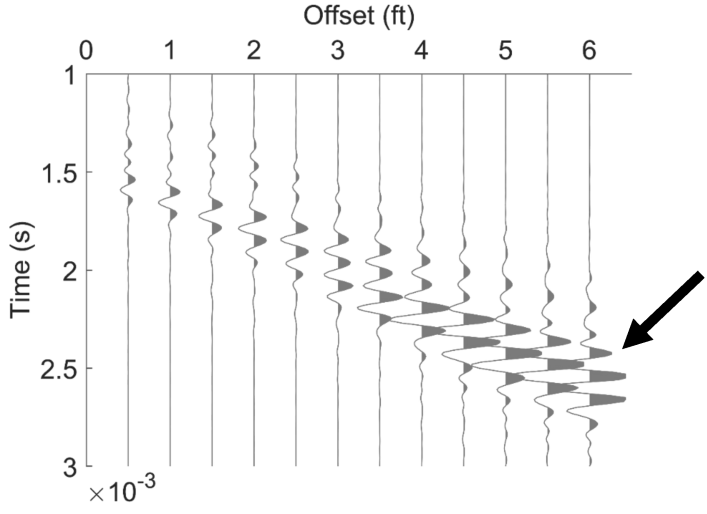

b) Super-virtual sonic waveforms using cross-coherence

Fig. 8. Field sonic data: a) SV sonic waveforms with deconvolution. b) SV sonic waveforms with cross-coherence. The solid arrow points to the sonic P-wave first arrivals and the spurious events caused by the cross-correlation datuming are suppressed. The far-offset first arrivals are enhanced and datuming with deconvolution and cross-coherence show the collapse of the spurious events that appears in conventional datuming by cross-correlation.

The effect of the various redatuming methods by cross-correlation, deconvolution, and cross-coherence are shown clearly in the corresponding cross-correlograms. Each cross-correlogram is obtain after the first datuming step by assembling all the virtual traces prior to stacking over the shots. Fig. 6a shows a cross-correlogram of a virtual shot response, obtained by the cross-correlation step. It clearly shows the alignment of the actual P-wave first-break after cross-correlation, marked by the black arrow. Each of the eight contributing shots along the integration surface S_0 is redatumed to the refractor at the virtual position and assembled in the cross-correlogram. Stacking these traces will coherently add the first-arriving P-wave that leads to the enhancement of its signal-to-noise ratio. However, the cross-correlogram is contaminated with spurious artifacts, marked by the dashed arrows. These can also add constructively and alter the resultant virtual response. This problem is alleviated by performing the first datuming step by deconvolution or cross-coherence as shown in the cross-correlograms in Fig. 6b and 6c. The spurious artifacts are severely suppressed and the virtual first-break response is aligned to yield the constructive interference after stacking over all shots.

FIELD DATA EXAMPLE

We demonstrate the method on a field dataset. The tool used to acquire the data consists of three monopole transmitters, namely upper and lower source with an offset range from 1 to 6 feet, and a far source with offsets from 11 to 17 feet. The tool contains 13 equally spaced receivers. The receiver interval is 0.5 ft, while the shot interval is also 0.5 ft. The larger number of receivers the larger the increase in SNR due to the increase in number of virtual sources. The time sampling rate of the sonic waveforms is 10 microseconds. The far transmitter enables the refracted wave to travel deeper in the formation, but the drawback is that its signal energy is weaker when it reaches the receivers on the tool. To demonstrate the effectiveness of the super-virtual sonic interferometry method on low SNR shot gathers we used the waveforms recorded by the far monopole source.

Fig. 7a shows raw waveforms. Note that the far receivers (i.e., receiver 8 and 13) have extremely low SNR making it difficult to visually identify the P-wave first break. To enhance the SNR, we apply the correlation-convolution super-virtual interferometric stacking and the results is plotted in Fig. 7b. Despite the enhancement of the P-wave first arrival (solid arrow) in the super-virtual sonic waveforms, the waveforms suffer from spurious events, which appears prior to the actual first arrivals (dashed arrow). To alleviate the artifact problem, we apply the SVRI method with deconvolution and cross-coherence, and plot the results in Figs. 8a and 8b, respectively. The spurious events prior to the actual first arrival waveforms are suppressed and the P-wave arrivals are enhanced, especially at the far-offset stations (solid arrow). The modified interferometric stacking also

demonstrates the suppression of the cross-correlation artifacts, in spite of the slight amplification of the noise prior to the first arrivals. The noise amplification level is tuned by the user depending on the choice of the value of ϵ. Due to the limited number of receivers of the sonic tool the fold obtained after each redatuming and stacking steps is limited compared to traditional surface seismic experiments. Despite the low fold inherent in the sonic tool geometry, real data examples clearly show a significant increase in SNR.

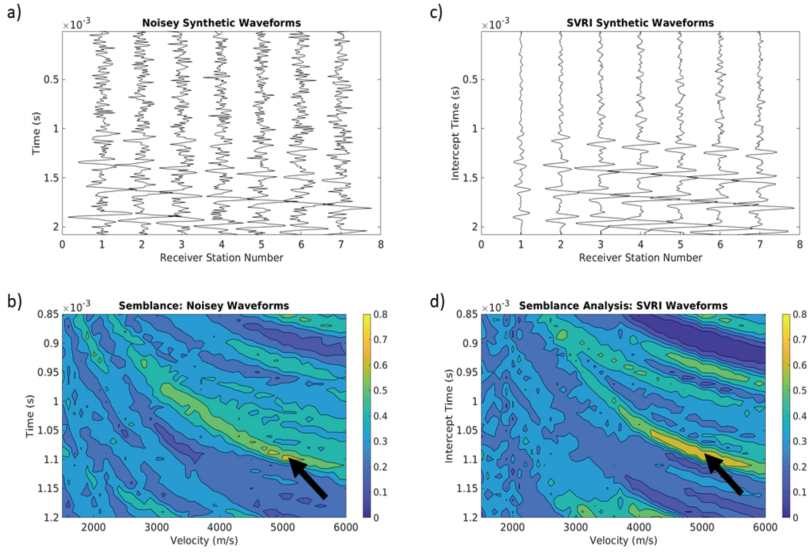

Fig. 9. Velocity analysis. a) Synthetic noisy sonic waveforms with SNT of 1.25. b) Semblance analysis of the synthetic noisy waveforms. The black arrow indicates the true velocity. c) The Synthetic SVRI waveforms. d) Semblance analysis of the synthetic SVRI waveforms. The black arrow indicates the true velocity.

VELOCITY ANALYSIS

The ultimate aim of sonic logs is to obtain accurate formation velocities (or slownesses). In this section, we analyze the effectiveness of the method in estimating interval velocities. We utilize a modified version of semblance analysis (Taner and Koehler, 1969; Alshuhail, 2011) to evaluate the quality of the velocities after applying SVRI. Note that our semblance analysis is targeted towards linear events such as first arrivals. Figs. 9a and 9c show the synthetic waveforms before and after SVRI while Figs. 9b and 9d show their associated semblance profiles. The peak, indicated with the

black arrow, is more clearly defined and distinguishable after applying SVRI. We then calculate the semblance profile for the field data. Figs. 10a and 10c show the field gathers before and after applying SVRI, respectively. Figs. 10b and 10d show the associated semblance profiles. The semblance profile in Fig. 10b shows few scattered peaks with similar energy (see at 2700 m/s and 4800 m/s). This may cause errors in identifying the formation velocity. The semblance profile after applying SVRI in Fig. 10d shows a more distinguishable peak and there are fewer peaks appearing at the higher velocities. The black arrows indicated where we picked the interval velocity in the semblance panel.

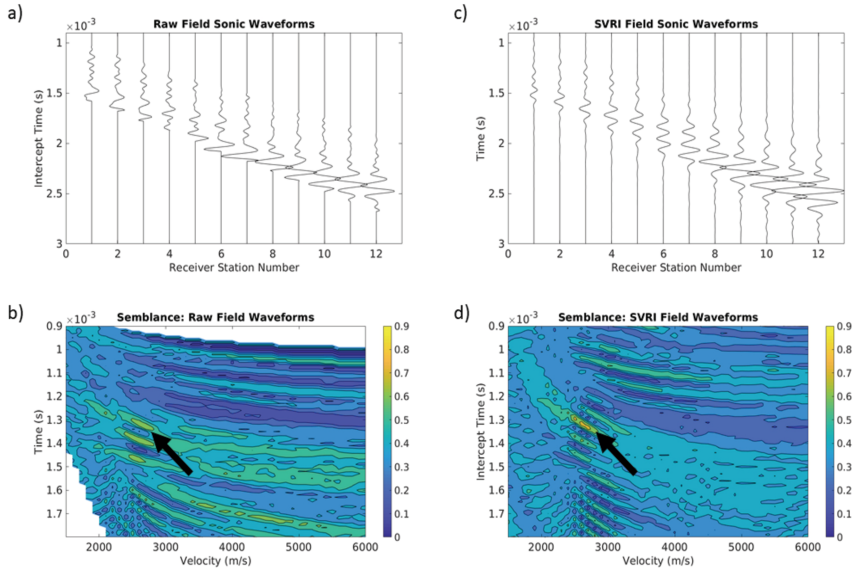

Fig. 10. Velocity analysis. a) Field sonic waveforms. b) Semblance analysis of the field waveforms. The black arrow indicates the velocity. c) The waveforms after applying SVRI. d) Semblance analysis of the SVRI waveforms.

CONCLUSIONS

Super-virtual refraction interferometry is a powerful tool that can be useful to increase the SNR in noisy environments. In this paper, we adapt the theory of super-virtual refraction interferometry so that it can handle refraction events in sonic waveforms. We applied the correlation-convolution super-virtual interferometric stacking to both synthetic and real data examples. The examples show a remarkable enhancement of the P-wave first arrivals in the super-virtual gathers of sonic waveforms. The resulting super-virtual gathers suffer from correlation artifacts and low

temporal resolution. We also noted that super-virtual datasets are polluted by spurious events prior to the actual P-wave first breaks. We therefore proposed a modified super-virtual interferometric stacking method by replacing the cross-correlation datuming step by a cross-coherence or deconvolution datuming step. Both the synthetic and field super-virtual sonic waveforms with cross-coherence or deconvolution show a notable enhancement of the P-wave first arrivals, and suppression of the correlation artifacts and spurious events. Cross-coherence or deconvolution datuming yield results with higher temporal resolution due to the deconvolution of the source signature. We finally applied a velocity analysis to estimate synthetic and field formation velocities before and after applying SVRI and concluded that SVRI can enhance the robustness of sonic waveform velocity analysis.

REFERENCES

Al-Hagan, O., Hanafy, S. and Schuster, G., 2014. Iterative supervirtual refraction interferometry. Geophysics, 79(3): Q21-Q30.

Alshuhail, A., Dawood, A.A. and Hanafy, S., 2012. Application of super-virtual seismic refraction interferometry to enhance first arrivals: A case study from Saudi Arabia. The Leading Edge, 31: 34-39.

Al-Shuhail, A, 2011. Estimation of direct-arrival velocity using the linear moveout velocity analysis method with application from eastern Saudi Arabia. J. Geophys. Engineer., 8: 524-530.

An, S., Hu, T., Liang, X. and Peng, G., 2014. Stable method to pick first-arrival refractions on undulating surface. Beijing Internat. Geophys. Conf. : 346-348.

Bendat, J.S. and Piersol, A.G., 2011. Random Data: Analysis and Measurement Procedures. John Wiley & Sons, New York, 729 pp.

Bensen, G.D., Ritzwoller, M.H., Barmin, M.P., Levshin, A.L., Lin, F., Moschetti, M.P., Shapiro, N.M. and Yang, Y., 2007. Processing seismic ambient noise data to obtain reliable broad-band surface wave dispersion measurements. Geophys. J. Internat., 169: 1239-1260.

Bharadwaj, P., Schuster, G., Mallinson, I. and Dai, W., 2012. Theory of supervirtual refraction interferometry. Geophys. J. Internat., 188: 263-273.

Chavez-Garcia, F.J. and Luzon, F., 2005. On the correlation of seismic microtremors. J. Geophys. Res., Solid Earth, 110: B11313.

Claerbout, J.F., 1992. Earth Soundings Analysis: Processing versus Inversion. Blackwell Science, Oxford.

Draganov, D., Campman, X., Thorbecke, J., Verdel, A. and Wapenaar, K., 2009. Reflection images from ambient seismic noise. Geophysics, 74(5): A63-A67.

Forghani, F. and Snieder, R., 2010. Underestimation of body waves and feasibility of surface-wave reconstruction by seismic interferometry. The Leading Edge, 29: 790-794.

Gao, H. and Zhang, J., 2017. 3D seismic residual statics solutions derived from refraction interferometry. Geophys. Prosp., 65: 1527-1540.

Goldberg, D., Guerin, G., Malinverno, A. and Cook, A., 2008. Velocity analysis of LWD and wireline sonic data in hydrate-bearing sediments on the Cascadia Margin. Proc. 6th Internat. Conf. Gas Hydrates, Vancouver, BC, Canada.

Guerin, G. and Goldberg, D., 2002. Sonic waveform attenuation in gas hydrate-bearing sediments from the Mallik 2l-38 research well, MacKenzie delta, Canada. J. Geophys. Res., Solid Earth, 107: EPM 1-1-EPM 1-11.

Guerin, G. and Goldberg, D., 2005. Modeling of acoustic wave dissipation in gas hydrate-bearing sediments. Geochem., Geophys., Geosyst., 6: Q07010.

Khadhraoui, B., 2011. Use of differential geometry properties for multichannel first break picking. Extended Abstr., 73rd EAGE Conf., Vienna.

Mallinson, I., Bharadwaj, P., Schuster, G. and Jakubowicz, H., 2011. Enhanced refractor imaging by supervirtual interferometry. The Leading Edge, 30: 546-550.

Milani, M., Rubino, J.G., Baron, L., Sidler, R. and Holliger, K., 2015. Attenuation of sonic waves in water-saturated alluvial sediments due to wave-induced fluid flow at microscopic, mesoscopic and macroscopic scales. Geophys. J. Internat., 203: 146-157.

Nakata, N., Snieder, R., Tsuji, T., Larner, K. and Matsuoka, T., 2011. Shear wave imaging from traffic noise using seismic interferometry by cross-coherence. Geophysics, 76(6): SA97-SA106.

Ruigrok, E., Campman, X., Draganov, D. and Wapenaar, K., 2010. High-resolution lithospheric imaging with seismic interferometry. Geophys. J. Internat., 183: 339-357.

Schuster, G.T., Yu, J., Sheng, J. and Rickett, J., 2004, Interferometric/daylight seismic imaging. Geophys. J. Internat., 157: 838-852.

Schuster, G.T., 2009. Seismic Interferometry. Cambridge University Press, Cambridge.

Snieder, R., 2004. Extracting the Green's function from the correlation of coda waves: a derivation based on stationary phase. Phys. Rev. E, 69: 046610, 1-8.

Snieder, R., Sheiman, J. and Calvert, R., 2006. Equivalence of the virtual-source method and wave-field deconvolution in seismic interferometry. Phys. Rev. E, 73(6): 066620.

Snieder, R., van Wijk, K., Haney, M. and Calvert, R., 2008. Cancellation of spurious arrivals in Green's function extraction and the generalized optical theorem. Phys. Rev. E, 78(3): 036606.

Taner, M.T. and Koehler, F., 1969. Velocity spectra - digital computer derivation and application of velocity functions. Geophysics, 34: 859-881.

Vasconcelos, I. and Snieder, R., 2008. Interferometry by deconvolution: Part 1: Theory for acoustic waves and numerical examples. Geophysics, 73(3): S115-S128.

Wapenaar, K. and Fokkema, J., 2006. Green's function representations for seismic interferometry. Geophysics, 71(4): SI33-SI46.

Wapenaar, K., Draganov, D., Snieder, R., Campman, X. and Verdel, A., 2010. Tutorial on seismic interferometry, Part 1: Basic principles and applications. Geophysics, 75(5): A195-A209.

Wapenaar, K., van der Neut, J., Ruigrok, E., Draganov, D., Hunziker, J., Slob, E., Thorbecke, J. and Snieder, R., 2011. Seismic interferometry by cross-correlation and by multidimensional deconvolution: a systematic comparison. Geophys. J. Internat., 185: 1335-1364.

Yu, J. and Schuster, G.T., 2004. Enhancing illumination coverage of VSP data by crosscorrelogram migration. Expanded Abstr., 74th Ann. Internat. SEG Mtg., Denver: 2501-2504.